5-22-2003

Lower Miocene to Present Stratigraphy of the Equatorial Pacific Sediment Bulge and Carbonate Dissolution Anomalies

Neil C. Mitchell
Cardiff University

Mitchell W. Lyle
Boise State University

Marie B. Knappenberger
Boise State University

Lee M. Liberty
Boise State University

 DOI: 10.1029/2002PA000828

Lower Miocene to present stratigraphy of the equatorial Pacific sediment bulge and carbonate dissolution anomalies

Neil C. Mitchell
Department of Earth Sciences, Cardiff University, Cardiff, Wales, UK

Mitchell W. Lyle, Marie B. Knappenberger, and Lee M. Liberty
Center for Geophysical Investigation of the Shallow Subsurface, Boise State University, Boise, Idaho, USA

Received 15 July 2002; revised 24 January 2003; accepted 18 February 2003; published 22 May 2003.

[1] The bulge is a 600-m-thick regional deposit of pelagic sediment accumulated around the equator. Its stratigraphy reflects a number of factors: how accumulation rates have varied over time, how accumulation has been spatially focused around the equator, how much carbonate dissolution and reworking or nondeposition by bottom currents have occurred, and how much the deposits have been translated northward by motion of the Pacific tectonic plate on which they have accumulated. In order to fully explore the effects of these processes, a spatially continuous stratigraphic database is desirable, as existing cores provide information at only discrete points, and they tend to be sited in locally thicker accumulations. We illustrate the utility of seismic data tied to drill cores by comparing the carbonate dissolution effect in two north-south lines crossing the sediment bulge. Bathymetry over our easterly seismic line deepens relatively little going north, whereas our westerly line deepens by 750 m from 4°N to 7°N. At a common latitude the primary pelagic input to both these lines will have been similar, so the difference of their sediment mass should reflect mostly their relative carbonate loss due to dissolution. We use this fact to calculate the slope of the carbonate dissolution curve and find a remarkably small slope (little relative carbonate dissolution) compared to that expected from previous studies. The techniques here may suggest a possible way forward for studying the equatorial carbonate stratigraphy more generally. *INDEX TERMS:* 4267 Oceanography: General: Paleoceanography; 3022 Marine Geology and Geophysics: Marine sediments—processes and transport; 3040 Marine Geology and Geophysics: Plate tectonics (8150, 8155, 8157, 8158); 4231 Oceanography: General: Equatorial oceanography; *KEYWORDS:* seismic stratigraphy, carbonate dissolution, carbonate compensation depth, Pelagic sediment redistribution, Pacific Deep Water, central equatorial Pacific

Citation: Mitchell, N. C., M. W. Lyle, M. B. Knappenberger, and L. M. Liberty, Lower Miocene to present stratigraphy of the equatorial Pacific sediment bulge and carbonate dissolution anomalies, *Paleoceanography*, *18*(2), 1038, doi:10.1029/2002PA000828, 2003.

1. Introduction

[2] The equatorial Pacific sediment bulge is a 600-m-thick deposit of pelagic carbonate and siliceous ooze and chalk elongated roughly parallel to the equator (Figure 1). The stratigraphy of the bulge idealized in Figure 2 reflects the combination of high equatorially centered pelagic sedimentation and the component of northward drift of the Pacific plate which have left a series of stratigraphic intervals displaced north of the equator [*Berger*, 1973; *Berger and Winterer*, 1974; *Lancelot*, 1978; *Leinen*, 1979; *van Andel et al.*, 1975; *Worsley and Davies*, 1979]. Sediments north of the equator at Deep Sea Drilling Project (DSDP) Sites 70, 71 and 161 progressively grade from nannofossil to radiolarian ooze away from the equator, with increasing carbonate dissolution and decreasing supply of pelagic sediment [*van Andel et al.*, 1975]. Because of the high sedimentation rates, the region's stratigraphy has attracted a great deal of interest as an important record of paleoceanography since (e.g.) *Arrhenius* [1963] onward. In a landmark paper, *van Andel et al.* [1975] analyzed all the information from DSDP cores to characterize systematically how sedimentation was focused about the equator as a result of the ocean upwelling system, how this focusing varied between different geological periods, how sedimentation fluctuated with geological time and how hiatuses apparently synchronous over large areas revealed regional nondeposition or erosion by corrosive deep bottom waters. Most of the more recent work has endeavored to understand this area at much finer temporal resolution in order to detect climate-related oceanographic events [e.g., *Mayer et al.*, 1992], although *Lyle* [2003] recently returned to study the long-term carbonate system using all the older DSDP core data along with more recent Ocean Drilling Program (ODP) cores. His study showed that much of the original work by *van Andel et al.* [1975] remains valid, but improved timescales now reveal that variations in carbonate mass accumulation rates are not synchronous across the whole Pacific basin and suggest that carbonate production in different parts of the Pacific has varied independently.

0883-8305/03/2002PA000828$12.00

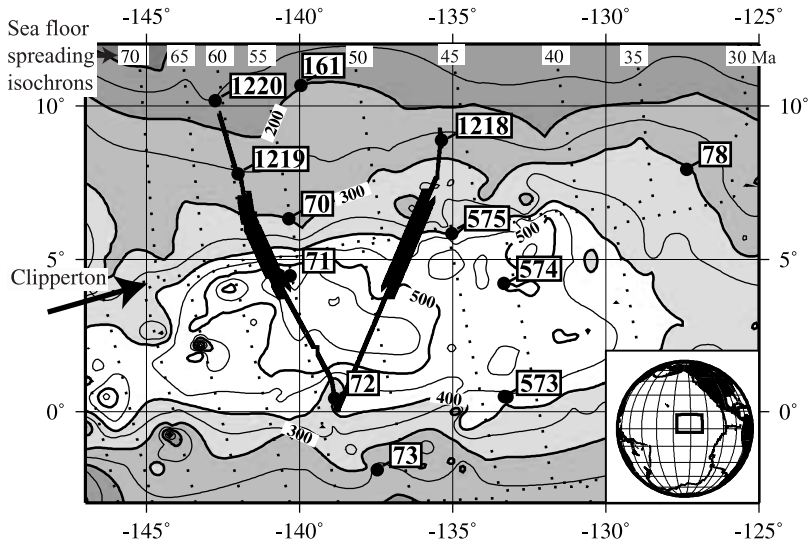

Figure 1. The location of the two R/V *Maurice Ewing* EW97-09 seismic reflection lines (bold) is shown over a map of contoured sediment thicknesses derived from seismic records [*Divins and Eakins*, 1997; *Mitchell*, 1998a]. The sediment thickness contour interval is 50 m with annotation every 100 m. The highlighted segments of the two bold lines locate the seismic data shown in Figure 8. The filled circles and associated bold, outlined numbers locate DSDP and ODP sites. Seafloor spreading isochrons from *Muller et al.* [1997] are shown with dotted lines and are annotated along the top of the map with ages in Ma. The region studied here shows a general decline in sediment thickness toward the north and over the Clipperton Fracture Zone (marked "Clipperton") which is used as a geographic reference in the text.

[3] Despite the undeniable progress that has been made by synthesizing the drill core data, more complete analysis would benefit from spatially continuous information, such as provided by seismic reflection data tied to drill sites, which then allow spatial variations in the system to be analyzed systematically [*Bloomer et al.*, 1995; *Lagos and Shipley*, 1989]. Seismic data are indeed routinely referred to in drill site selection but only rarely are they used in an integrated way with core data. The problem is illustrated in Figure 3a in which interpreted seismic two-way travel time (TWT) for sediment overlying the 20 Ma reflector of our westerly line is plotted against latitude. The sediment cover fluctuates greatly over short distances, a feature that we ascribe mostly to local effects, such as due to transport of sediment off local highs and erosion or nondeposition effects of spatially variable geostrophic and tidal currents.

[4] To illustrate the spatial scale of this variability, we assume that the data have a short-wavelength stochastic component (i.e., the local fluctuations) and a long-wavelength systematic component [*Mitchell*, 1998b], which we here approximate by the polynomial in Figure 3a. This is a simplification because in reality most processes act over a wide range of scales, but some processes might be expected to dominate short length scales, e.g., nondeposition by tidal currents acting over the crests of abyssal hills will have a length scale reflecting the spacing of hills. For the large-scale systematic component, individual "event" deposits such as diatom mats [*Kemp et al.*, 1995] may have abrupt boundaries, but variability in the extents of many such deposits is likely to lead to smooth, gradual spatial variation in primary input for the 0–20 Ma sediments as a whole. The stochastic variability can be characterized by filtering the data over progressively longer length scales and observing the change in root-mean squared (RMS) variation about the polynomial. The result of such a procedure in Figure 3b shows a rapid decline in RMS from R1. With heavy smoothing (filter width >2°) the RMS variation (R0) is small and flat so most local variability is then removed. We suggest that 1° of latitude is a useful measure of the short-wavelength fluctuation length scale here, because the RMS variation is reduced to 23% of R1-R0 (R0.23) when the data are filtered over 1°. According to this measure, for any drill site accumulation rate data to be truly representative of their locales, they should be adjusted for local effects using seismic data over an area of at least 100 km across.

[5] The classical carbonate dissolution model is illustrated in Figure 4, in which carbonate mass accumulation rates (MARs) vary linearly with depth from a carbonate lysocline down to the Carbonate Compensation Depth (CCD) [*Berger et al.*, 1982; *Peterson*, 1966]. Above the lysocline, carbonate MARs are relatively unaffected by differences in depth, whereas below the CCD the sediments are carbonate free (near zero carbonate MAR). Between the lysocline and CCD, the rate of change of carbonate MAR with depth has been termed the "dissolution rate gradient" [*van Andel et al.*, 1975]. *van Andel et al.* [1975] and *Heath et al.* [1977] inferred these gradients from differences in carbonate MAR between central Pacific DSDP sites and Figure 5 shows how these gradients varied with time [*Heath et al.*, 1977]. Plots of carbonate MAR versus paleodepth for different age intervals

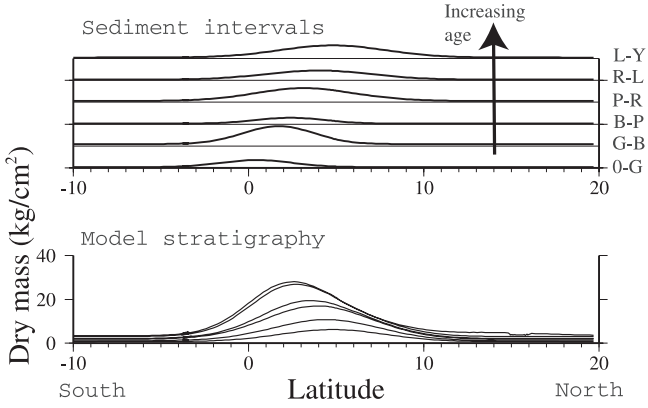

Figure 2. Idealized stratigraphy for a north-south line through the equatorial Pacific sediment bulge. The lower graph shows the 0–20 Ma stratigraphy (in terms of sediment dry mass per unit area), and the upper graphs show the individual sediment intervals. The thickest sediment in each of these intervals is displaced north of the equator reflecting the amount of plate drift for the particular age of sediment (the *Sager and Pringle* [1988] apparent polar wander path was used to predict the latitudinal drift due to plate motion, which is 30 km/Ma in this area of the central Pacific). The sediment distribution was created using the numerical model in Figure 14 (without adjustments for varied carbonate dissolution with depth) for a transect corresponding to the 56-Ma seafloor isochron shown in Figure 1. The annotation represents sediment isochrons corresponding to the ages of seismic reflectors green (G), brown (B), purple (P), red (R), lavender (L) and yellow (Y) of *Mayer et al.* [1985].

showed remarkably simple linear trends [*Heath et al.*, 1977], supporting the classical dissolution model (Figure 4). Surprisingly, although this model found favor after the pioneering work of the 1970s, with a few exceptions [e.g., *Berger and Stax*, 1994] there has been relatively little attempt to test it.

[6] Outside the central equatorial region (±4° of latitude), the dependence of dissolution rate on depth was derived [*Heath et al.*, 1977] from cores alone and largely excluding the northwest flank of the sediment bulge because only one deep site (DSDP Site 70) exists in this area to characterize the trend. In the more recent literature, the rate of carbonate burial and preservation is described as a complex function of the rates of supply of calcite and of organic matter, which degrades to produce corrosive pore waters [*Archer*, 1991], size fraction of the carbonate material [*Berger et al.*, 1982] and the degree of calcite undersaturation of bottom waters. Kinetic factors are also important [*Thunell et al.*, 1981], as illustrated by observations of eroded carbonate strata with no sign of locally redeposited erosion products, and where the eroded areas appear to occur where bottom currents are enhanced by the seabed topography [*Johnson*, 1972; *Mayer*, 1981]. Given these potential complications, it is a timely point to re-evaluate the classical model in the light of the new seismic and core data.

[7] Our working model used to extract information on carbonate dissolution is illustrated in Figure 6, in which 'A' and 'B' represent our westerly and easterly seismic lines, respectively. Running north from the equator, individual stratigraphic intervals should progressively thin because of (1) decreasing primary input and (2) increasing dissolution as the bathymetry deepens along these lines as shown in Figure 7. Equatorial productivity can be assumed to be nearly one-dimensional west of ~110°W [*Chavez and Barber*, 1987] so that the primary input for a given latitude will have been the same for the two lines (i.e., they have the same 'm0' in Figure 6b). In this model, the only major difference in carbonate accumulation rate (Δm) between the lines arises from their different depths Δz. By working out the mass interval between stratigraphic horizons (ΔM = Δm*age interval) we can therefore easily calculate the dissolution rate gradient (Δm/Δz). At a different latitude, m0 will be different but the ratio of Δm to Δz should be the same if the

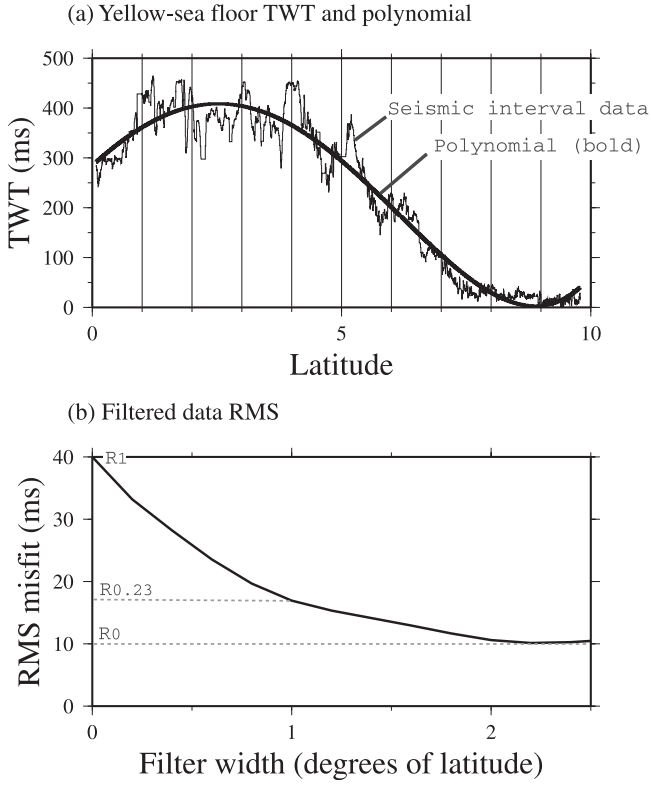

Figure 3. (a) The seismic two-way time for the sediment overlying reflector "yellow" is shown against latitude, to illustrate the variability in the data over short length scales. The bold curve is a fifth-order polynomial fitted to the data [*Wessel and Smith*, 1991] to represent its long-wavelength systematic component. (b) The spatial scale of the variability is characterized by filtering the data in Figure 3a over progressively larger length scales and calculating its root-mean squared (RMS) variation R relative to the polynomial. With very heavy smoothing (filter width >2°) the RMS variation (R0) is small and flat so most variability is removed. When the data are filtered to 1° of latitude, the RMS variation is reduced to 23% of R1-R0 (R0.23), and most variability is removed. This 1° length scale therefore roughly represents the short-wavelength fluctuation of the data.

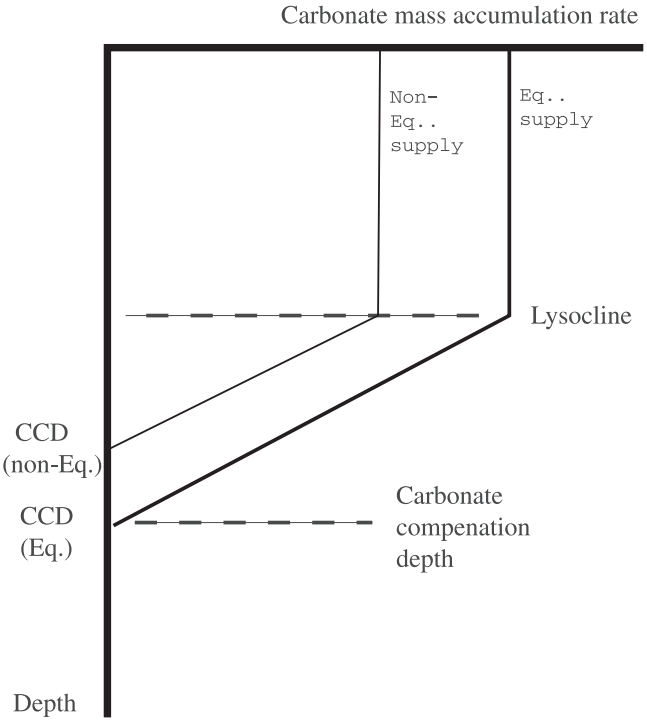

Figure 4. The classical model for carbonate mass accumulation rates modulated by dissolution at the seafloor. In this model, carbonate mass accumulation rates vary linearly between a CCD and a lysocline. Below the CCD, negligible carbonate accumulates, whereas above the lysocline the carbonate mass accumulation rates vary negligibly with depth and has a value determined by the primary input. If the rate of change of carbonate accumulation with depth below the lysocline and the lysocline depth are constant, a change in primary input causes the CCD to change (hence the different CCD for equatorial and nonequatorial regions shown).

dissolution rate gradient is uniform and if the paleoseabed lay between the CCD and the lysocline. An array of (ΔM, Δz) values from different latitudes can therefore be obtained to constrain this gradient. Although this procedure might at first seem to assume the model in Figure 6b, we show that it also allows us to test the model assumptions such as uniform dissolution rate gradient and equal m0 between the lines at a constant latitude. The following paper describes the seismic data and conversion of seismic intervals to sediment mass before describing the principal results, which are the regional mass accumulation rate curve for the central Pacific and the dissolution rate gradients.

2. Seismic Data

[8] Seismic reflection data in the central equatorial Pacific have a remarkable acoustic stratigraphy, with reflectors traceable for more than a thousand kilometers [*Bloomer et al.*, 1995; *Mayer et al.*, 1986]. *Mayer et al.* [1986] identified reflectors associated with changes in carbonate content in the equatorial sediments drilled on DSDP Leg 85 at Site 574 (Figure 1). They suggested that major paleoceanographic events caused the impedance contrasts of these reflectors and that the seismic reflectors are chronostratigraphic. At least two of these reflectors were identified in the eastern equatorial Pacific in sediments recovered by Leg 138 at 110°W [*Bloomer et al.*, 1995], providing support for their chronostratigraphic nature and illustrating their widespread occurrence. We have used this chronostratigraphic character to map variations in sediment intervals across the central and northern regions of the equatorial sediment bulge, along two seismic lines tied to DSDP and ODP sites.

[9] The seismic reflection data were acquired on the EW9709 cruise of the R/V *Maurice Ewing* as part of a survey of potential drill sites for ODP Leg 199 [*Lyle et al.*, 2002b]. Most of the data were recorded while the ship was underway between sites at 10 knots using an 80 cubic inch water gun as the seismic source. They were recorded on the *Ewing's* Digicon seismic acquisition system using a 2 msec sample spacing. An analog high-cut filter at 180 Hz was in place during recording. Because of the high speed along the transect, significant noise was generated by the streamer ("strum") at around 15–20 Hz, which was filtered out using an aggressive low-cut filter. The data shown (Figure 8) are stacked and migrated 4-channel data processed using Landmark's ProMax™ software. The data processing is

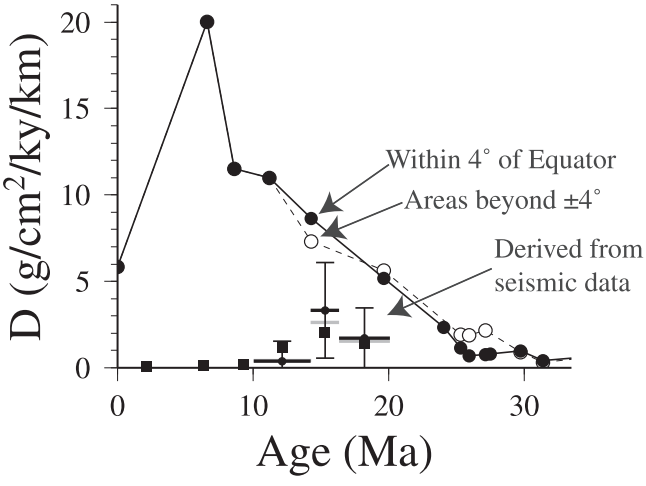

Figure 5. The graph shows the rate of change of carbonate MAR with depth below the lysocline [*Heath et al.*, 1977] (solid circles represent rates calculated for areas within 4° of the paleoequator and open symbols are from outside the ±4° equatorial region). Values and dates have been adjusted to the *Cande and Kent* [1995] timescale. The horizontal bars show estimates of dissolution rate gradients made from the *Ewing* seismic data using the dashed regressions in Figure 13 (the gray bars show values derived from similar regressions on basement depth differences to illustrate uncertainty). The bar horizontal extents represent the age intervals whereas the associated vertical bars represent the combined uncertainty (2σ) in D of the regression coefficients and of the reflector ages in Table 1. The solid squares show the corresponding rates from the difference in carbonate mass between DSDP Sites 575 and 70 in Figure 12 and verify the seismic-derived results.

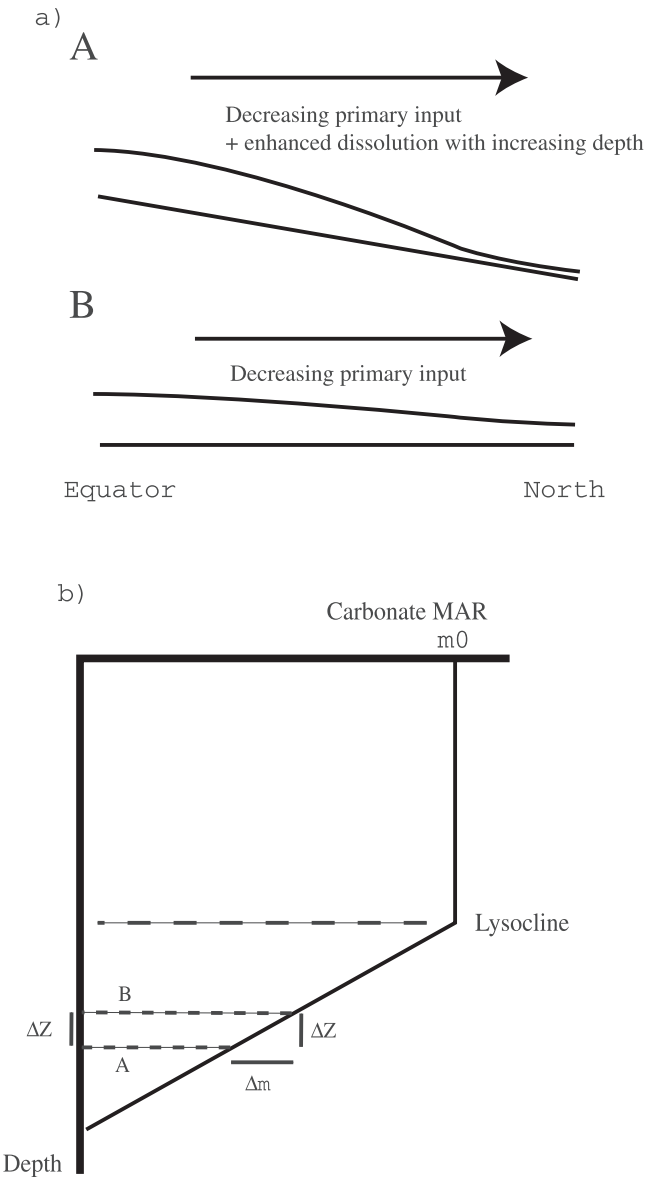

Figure 6. (a) The change in sediment mass expected to be caused by primary input and dissolution is shown for the two seismic lines (A, westerly line; B, easterly line). Both lines experience the same decreasing primary input away from the equator but line A would be expected to experience greater carbonate dissolution because of its greater deepening bathymetry going north. (b) For any given latitude the primary input to both lines is the same (equal m0) but their depth differences Δz lead to a different carbonate accumulation rate Δm. In the study here the seismic data are used to derive the slope Δm/Δz. Data from different latitudes will have different m0 but still the same Δm/Δz if the dissolution rate gradient is uniform and if the dissolution model were correct. Constructing graphs of Δm (differences of stratigraphic mass interval between the lines) against Δz carried out here (1) tests whether the dissolution rate gradient is regionally uniform, (2) allows us to derive its magnitude and (3) tests whether m0 is uniform for a given latitude.

described more fully elsewhere [*Lyle et al.*, 2002a] but essentially involved bandpass filtering, stacking, and F–K migration assuming a constant 1500 m/sec P wave velocity.

[10] Distinctive reflection sequences were interpreted from both these lines [*Knappenberger*, 2000]. For consistency with earlier work, the same reflectors as identified by *Mayer et al.* [1985] were identified and mapped. We also used Mayer et al.'s nomenclature, with reflectors assigned the colors green to yellow as given in Table 1, and with corresponding dates revised to account for more recent biostratigraphy and magnetostratigraphy [*Lyle et al.*, 2002a]. The upper two graphs in Figure 9 show the seismic two-way times (TWT) of the reflectors referenced to the deepest (yellow) reflector and the second row of graphs show the same reflector TWTs after filtering the data to make them more easily interpretable.

2.1. Conversion of Seismic TWT to Sediment Mass

[11] We calculated the sediment dry mass per unit seafloor area for individual seismic intervals as follows. The seismic TWT of reflectors was first converted to depth below

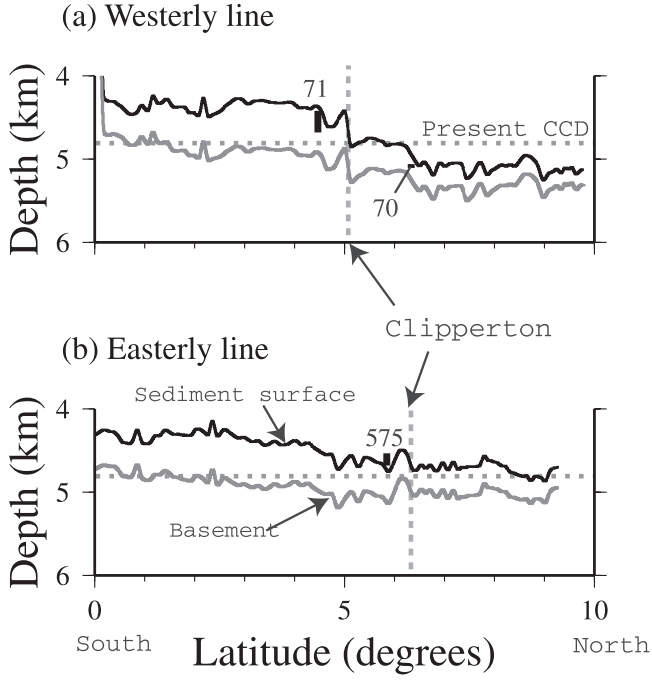

Figure 7. Regional bathymetric sections along the two *Ewing* seismic lines shown in Figure 1. Because the basement was difficult to interpret from the seismic data, the basement depth shown (bold gray lines) was constructed by subtracting the regional sediment thickness from the bathymetry [*Divins and Eakins*, 1997; *Mitchell*, 1998a] (note that there are differences with Figure 8 because these represent regionally averaged data). The vertical gray dashed lines show the approximate location of the Clipperton Fracture Zone and the horizontal dotted lines show the modern regional CCD at around 4800 m derived from core top carbonate compositions [*Berger et al.*, 1976]. DSDP Sites 70, 71 and 575, which lie close to the two seismic lines, are shown with their depth extent of drilling.

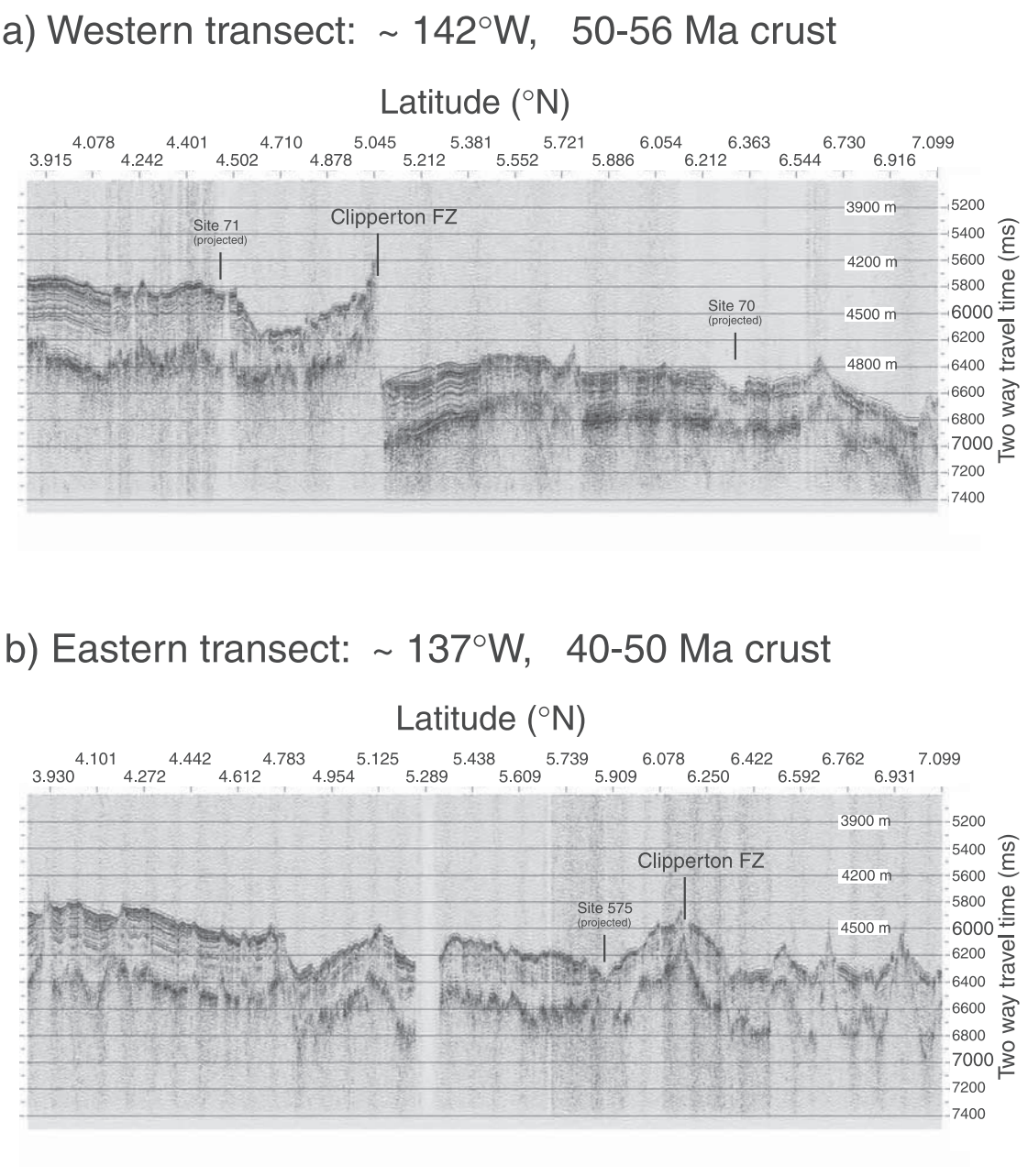

Figure 8. Examples of processed seismic data from R/V *Maurice Ewing* cruise EW97-09. The two sections are located in Figure 1.

seafloor using a look-up table calculated from a seismic velocity model [*Mayer et al.*, 1985] in which velocity varies with depth z below the seabed according to:

$$V(z) = 1523.9 + 0.5476z + 0.00091509z^2. \quad (1)$$

Depth was then converted to cumulative sediment dry mass per unit seafloor area using the following relationship for dry bulk density ρ derived from DSDP Leg 85 physical property data [*Mitchell*, 1998a]:

$$\rho(z) = 0.61758 + 0.000424115z - 5.56148.10^{-6}z^2. \quad (2)$$

The results are shown in Figure 10 as the sediment dry mass versus latitude for the stratigraphic intervals (the dashed and continuous lines represent the westerly and easterly lines, respectively).

2.2. Interpretation of the Seismic Data

[12] The identified horizons (Figure 9, top graphs) show a great deal of variability that reflects variations in local deposition [*Knappenberger*, 2000]. The variation is primarily related, not to seamounts or other large topographic features, but instead to the crossing of the more subdued abyssal hill topography. There is a consistent trend of greater deposition in the basins compared with the topo-

Table 1. Interpreted Seismic Horizons Based on the Nomenclature of *Mayer et al.* [1985]

Reflector Name	Radiolarian Zone	Age,[a] Ma
Green	*S. pentas*	4.2 (3.8–4.6)
Brown	*D. Pentultiima*/*D. Antepenultima*	8.55 (8.3–8.8)
Purple	*D. Pettersoni*	10.05 (9.6–10.5)
Red	*D. Alata*	14.25 (13.5–15.0)
Lavender	*C. Costata*	16.35 (15.7–17.0)
Yellow	*S. Delmontensis*/*C. Tetrapera*	20.1 (19.7–20.5)

[a]Stratigraphic age of the reflectors of *Mayer et al.* [1985] with dates updated using a recalibrated radiolarian biostratigraphy reconciled with magnetostratigraphy for ODP Leg 199 [*Lyle et al.*, 2002b]. Age range in brackets represents conservatively the combined uncertainty in the age scale, sampling down core and the core-seismic correlation [*Mayer et al.*, 1985].

graphic highs as found elsewhere [*Lagos and Shipley*, 1989].

[13] Figure 9 along with the bathymetry in Figure 7 illustrate our point that carbonate dissolution has not reduced accumulation rates in simple proportion to depth differences. The westerly line has a large bathymetry range from 5°N to 7°N, more than double that of the easterly line, but the thinning of the 0–20 Ma stratigraphy is if anything greatest for the easterly line. The present-day bathymetry deepens by 750 m from 4°N to 7°N for the westerly line in Figure 7. Assuming a dissolution rate gradient of ~10 g/cm^2/kyr/km (Figure 5) and a dry sediment density of 1 g/cm^3, these differences in depth should have led to up to 750 m difference in sediment thickness over 10 Ma, or differences of seismic TWT of up to 850 msec (at 1800 m/s seismic velocity). This dramatic thinning is clearly not observed. This point is reinforced by Figure 10 in which the sediment mass north of 6°N deposited from 14.25 Ma to present is smallest along the easterly line, rather than along the westerly line as would be expected from its deeper bathymetry. We note further that the shallower bathymetry of the easterly line coincides with a bend of the Clipperton fracture zone, implying that it originates from process that occurred at or near the ancient East Pacific Rise rather than much younger.

2.3. Plate Motion Effect

[14] Whereas the center of the purple-brown interval (8.55–10.05 Ma) lies closer to the equator than the older intervals (Figure 10), there is only a weak northward progression of the center of sedimentation in the older intervals, a feature that we ascribe to distortion of the depositional pattern by carbonate dissolution. The progression expected from current models of Pacific plate motion [*Knappenberger*, 2000] is illustrated in Figure 2. An alternative interpretation is that this lack of progression is evidence for error in the plate motion model [*Knappenberger*, 2000]. Indeed, plate motions derived from paleomagnetic poles have typical standard errors of 2°–4°[*Sager and Pringle*, 1988] and could readily accommodate significant latitude error. Motions deduced from hotspot trails are also compromised by concerns that the hotspots may not provide a reliable reference frame for the bulk earth and, for the Pacific in particular, whether the 5 Ma and other bends in the Hawaiian chain represent changes in hotspot or plate motion [*Tarduno et al.*, 2001; *Wessel and Kroenke*, 1997]. Hotspot-deduced motions thus also have large standard errors. We note that the sedimentary depocenter appears displaced by 2° south of the hotspot-predicted location at 18 Ma [*Knappenberger*, 2000] and therefore an error of 3°–4° of latitude at 30–40 Ma would be expected if this trend continued. The ODP Leg 199 data, however, located the paleoequator to <2° of hotspot prediction during this time interval [*Lyle et al.*, 2002b], suggesting that plate model error is minor. Furthermore, the center of equatorial deposition for the 110°W transect drilled during ODP Leg 138, where carbonate dissolution is less important, shows the expected simple paleolatitude trend with <1° of latitude deviation for 0–10 Ma [*Mitchell*, 1998a]. The plate models therefore seem reasonable and the lack of northward progression in the position of the depocenter more likely reflects other causes, such as erosion and nondeposition by bottom currents and/or depth-dependent carbonate dissolution being controlled by the bathymetric variation. These effects distort the deposited sediment sequence and make the paleoequator difficult to interpret from seismic thicknesses alone.

3. Regional MAR of the Central Equatorial Pacific

[15] The regional MARs shown in Figure 11 (bold lines) were produced by averaging the interval masses over 0°–5°N and dividing by their age ranges (Table 1). The graphs both reveal a general decline in regional MAR toward the present. The gray areas in Figure 11 represent uncertainty in MAR based on the extremes of the age ranges in Table 1. Whereas these uncertainties are somewhat conservative, they suggest that the step change in MAR at around 15 Ma is poorly resolved. The change at around 9 Ma is resolved, however, and occurred only 1 Ma after a steep decline in carbonate deposition in the eastern equatorial Pacific [*Lyle et al.*, 1995]. It occurred at a similar time to the Panama gateway closure but a strong explanation for such a link is unclear at present.

[16] Whereas the general decline since 14 Ma may partly reflect the drift of the paleoequator, e.g., from around 2.5° N at 10 Ma [*Mitchell*, 1998a] when sedimentation would have been nearly centered over the 0°–5°N region, the decline should be more gradual and much smaller in magnitude than shown in Figure 11. In addition, a prominent peak in MAR occurs at around 5–6 Ma at the ODP Leg 138 equatorial sites (110°W) [*Farrell et al.*, 1995; *Lyle*, 2003], but there is no evidence of such large MARs during the corresponding 4.2–8.6 Ma period in Figure 11; previous claims to correlate this peak were probably artifacts of timescale error [*Lyle*, 2003]. Such difficulties in correlating core data demonstrate the need for further work integrating core and seismic data to develop more accurate sedimentary models of the central Pacific.

4. Calculating Dissolution Rate Gradients

[17] We now return to the objective of deriving the rate of dissolution with depth illustrated in Figure 6. As mentioned

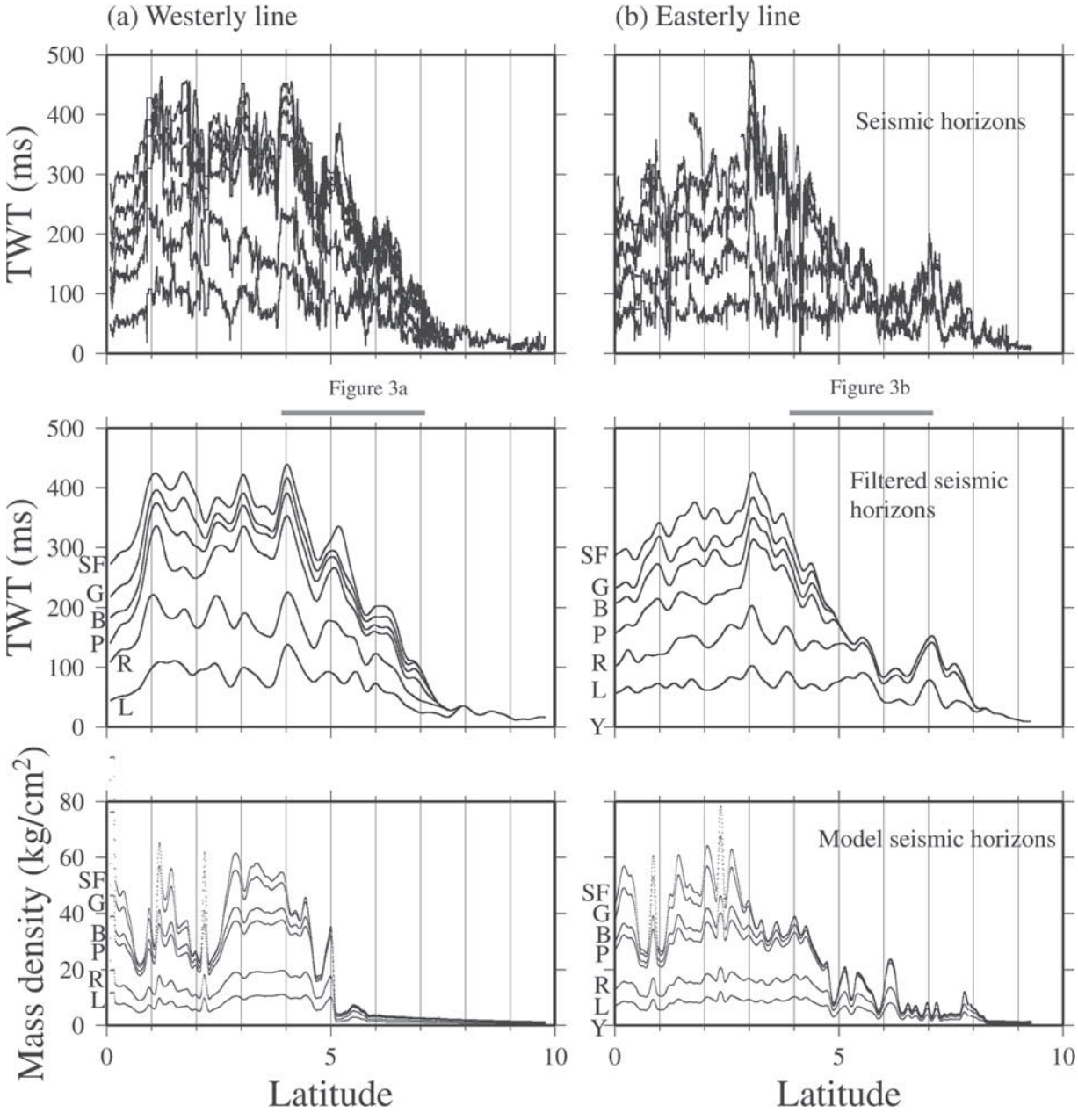

Figure 9. The stratigraphy derived from the *Ewing* seismic records (top two graphs) is shown along with that predicted by the numerical model (lower two graphs). The middle graphs show the seismic two-way travel time (TWT) smoothed to reduce fluctuations using a cosine tapered filter of full width 0.5° of latitude. Note that the model output is in sediment dry mass per unit area, whereas the seismic-derived data are in seismic TWT in msec (in practice there are no major distortions between these two types of data so they can be broadly compared). Both the seismic-derived data and the model are referenced to the 20.1 Ma sedimentary isochron (i.e., seismic TWT relative to the yellow horizon and mass density to sediment of that horizon's age). The annotation represents seismic reflectors green (G), brown (B), purple (P), red (R), lavender (L) and yellow (Y) of *Mayer et al.* [1985], and SF represents the seafloor. The gray bars below the top two graphs locate the sections in Figure 8.

earlier, the difference in sediment mass between the two seismic lines at a common latitude should predominantly reflect differences in carbonate dissolution because the primary input will have been similar owing to the one-dimensional structure of pelagic productivity [*Honjo et al.*, 1995].

[18] For each of the two seismic lines, the sediment mass intervals (Figure 12) and the corresponding bathymetry

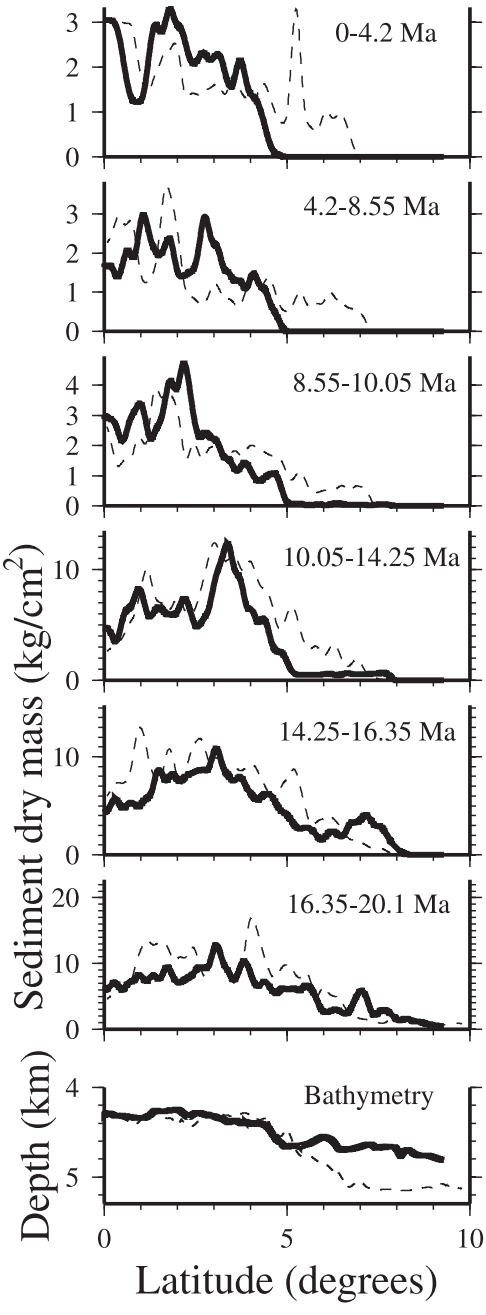

Figure 10. The sediment distribution of individual age intervals in Figure 9 (middle graphs) are shown converted to sediment dry mass per unit area. The dashed lines show results from the westerly seismic line and the bold lines for the easterly line. Also shown is the corresponding bathymetry for these lines (bottom graph).

were averaged over 1.0° of latitude, a length scale that will remove most local variability (Figure 3). The differences of these depth averages (Δz) and of the sediment mass averages (ΔM), calculated at common latitudes, are shown in Figure 13. (Graphs produced using basement depth as the variable were very similar to Figure 13 and differences in either bathymetry or basement depth approximate differences in true paleodepth because subsidence was shallow for 0–20 Ma (Figure 14c).) The data from 0°–5°N are shown in Figure 13 as unfilled circles and those north of 5°N as filled circles. The continuous lines show regressions through all the data for each of the periods 10–20 Ma. We also calculated the following value (correlation coefficient) from the data in Figure 13;

$$R = \frac{\sum((x_i - < x >)(y_i - < y >))}{\sqrt{\sum(x_i < x >)^2 \sum(y_i - < y >)^2}}, \qquad (3)$$

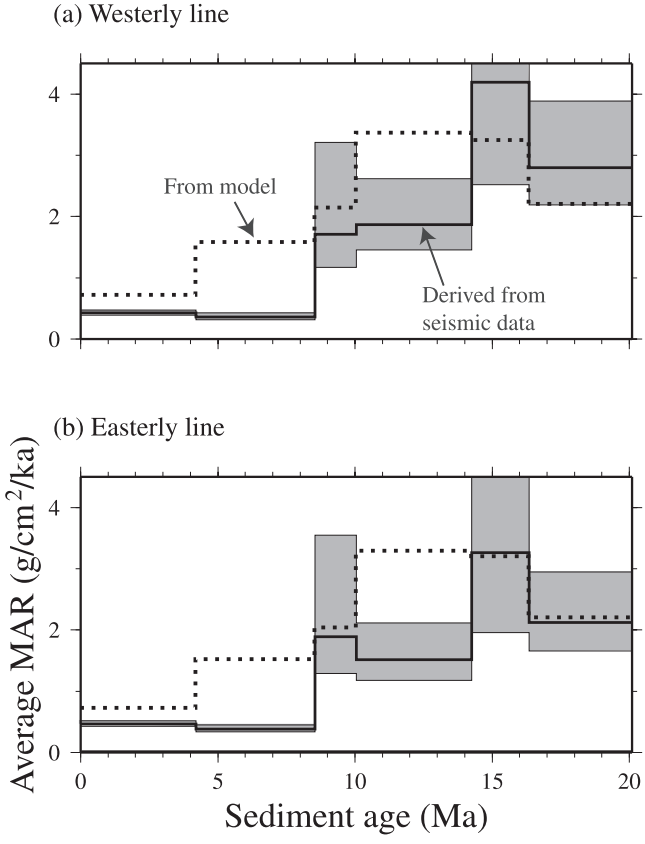

Figure 11. The variation in the central equatorial Pacific regional mass accumulation rate (MAR) with age. The MARs derived from the seismic data (bold lines) were calculated by averaging the dry sediment mass between particular seismic intervals (Figure 12) over the region 0°–5°N and dividing by their age intervals (Table 1). The gray shading represents effect of uncertainties in the reflector dates and was derived using the extremes of the age ranges in Table 1. The dotted lines show the corresponding MAR in the model calculated from the results shown in the lower graphs in Figure 9. Both the data and model show a declining MAR toward the present day but the model MAR is generally too large during 4–14 Ma and also has a different shape. This indicates that the MAR data for DSDP Sites 573 and 574 are anomalously high, probably owing to locally enhanced sedimentation at those sites, and also that they do not accurately represent how sedimentation has varied over time at the regional scale.

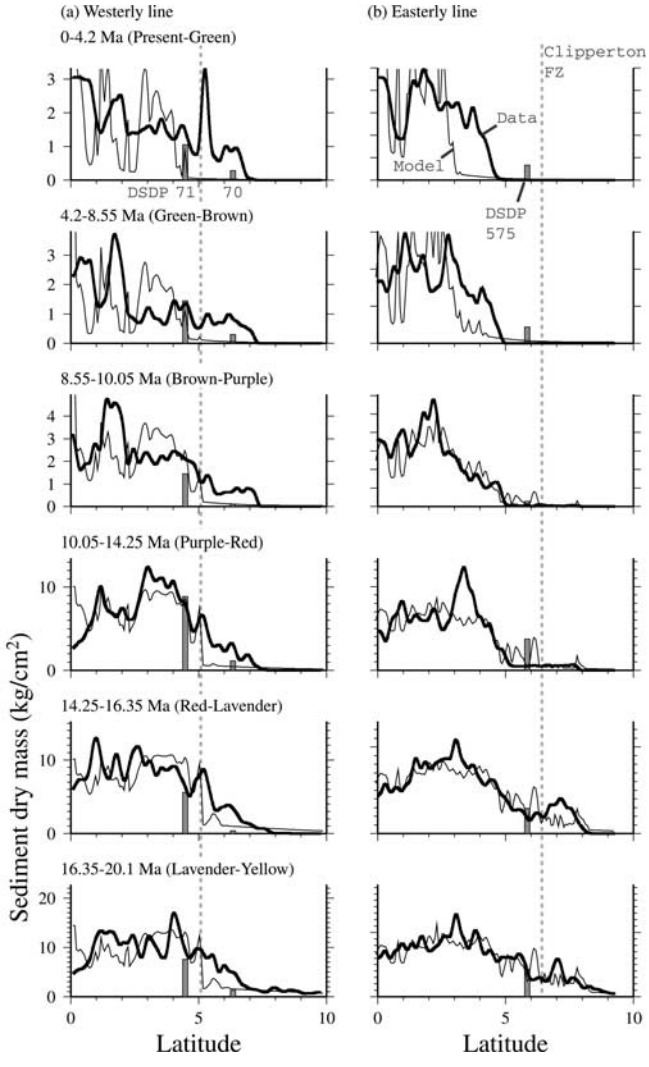

Figure 12. The bold lines show the sediment mass distributions of Figure 10 to compare against corresponding intervals in the numerical model (fine lines, derived from the lower graphs in Figure 9). Because of discrepancy in the total mass between the model and the seismic-derived data for some stratigraphic intervals, the model sediment mass has been rescaled to the same mean value as the data over 0°–5°N, so that the shapes of the intervals can be compared. The vertical gray dashed lines locate the Clipperton Fracture Zone. Also shown by the vertical gray bars are the dry sediment mass for these age intervals in the nearby DSDP Sites 70, 71 and 575.

where x_i and y_i are the ordinate and coordinates of the data and $\langle x \rangle$ and $\langle y \rangle$ are their means. The data in the three graphs for 0–10 Ma showed no correlations ($|R| < 0.2$), while the three graphs for 10–20 Ma showed weak correlations ($R = 0.24$ for 14.25–10.05 Ma, 0.74 for 16.35–14.25 Ma and 0.61 for 20.1–16.35 Ma).

[19] If the dissolution rate gradients were uniform across the region, each graph of ΔM and Δz data should show a linear array of constant slope proportional to the dissolution rate gradient ($\Delta m/\Delta z$) and the trend should pass through (0,0). The dashed lines, for example, show the trends expected from the gradients of *Heath et al.* [1977] in Figure 5 and clearly the data do not readily conform to them.

[20] The lack of a trend for 0–10 Ma probably reflects the fact that areas on the north side of the sediment bulge were close to or below the CCD for much of this time and sedimentation rates were generally very low. Figure 15b, for example, shows nearly zero carbonate content for DSDP Site 70 and intermediate carbonate for Site 575, indicating

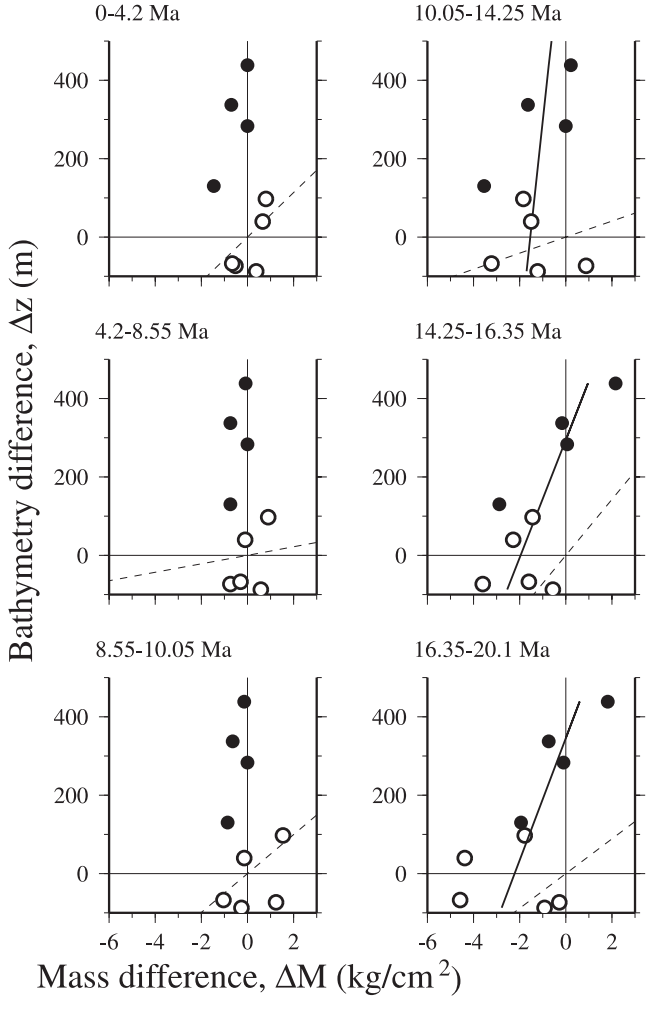

Figure 13. For each age interval the graphs show the difference in dry sediment mass ΔM (calculated from the data in Figure 12) of the two seismic lines at a common latitude plotted against their difference in bathymetry Δz. Each data value was calculated by averaging the sediment mass and depth over 1.0° of latitude, and then differencing these average values between the two lines. Each pair of ΔM and Δz defines the gradient of the carbonate MAR curve; a uniform dissolution rate gradient with depth across the region should lead to straight-line graphs. The dashed line shows the trend predicted by the dissolution rate gradients in Figure 5. The solid lines in the three graphs for 10–20 Ma are least squares regressions. Unfilled circles represent values from south of 5°N.

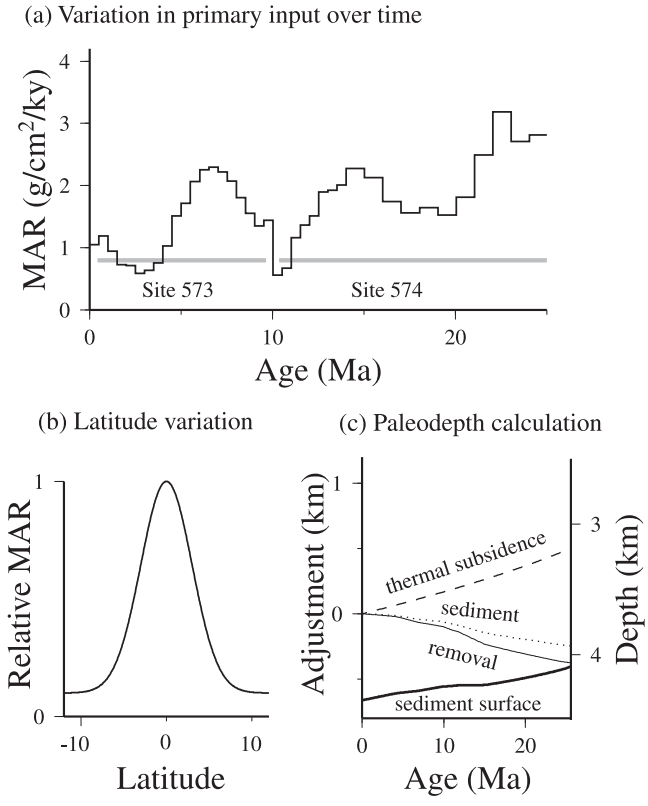

Figure 14. Components of a numerical model [*Mitchell*, 1998a] used to illustrate aspects of the carbonate system. (a) Mass accumulation rates (MARs) for DSDP Sites 573, 573B, 574 and 574C [*Lyle*, 2003] (a rate of 0.5 g/cm^2/kyr was used beyond 25 Ma, an average value from *van Andel et al.* [1975]). These were used first to define the regional MAR at a given time in the model. (b) To account for equatorial concentration of sediment supply, the MARs of Figure 14a were adjusted using this Gaussian function and a calculated paleolatitude. (c) Example calculation of paleodepth (bold line), which was used to adjust the rates derived from Figures 14a and 14b for differences in carbonate dissolution with depth. The evolution of the sediment surface was calculated by allowing for lithosphere thermal subsidence (dashed) and for effect of stripping off successive surficial sediment layers (fine continuous line), also allowing for isostasy (dotted line). Due to competition between thermal subsidence and sediment accumulation, the evolution for sites of thickest sediment can be significantly flatter than predicted by the subsidence alone.

extensive dissolution in areas close to the seismic lines (Figure 1). The modern CCD derived from surface sediment carbonate contents also lies at around 4800 m [*Berger et al.*, 1976], marked by the horizontal gray dotted lines Figure 7.

[21] The older 10–20 Ma sediments, however, had more significant carbonate content (Figure 15b) and for this age interval the graphs in Figure 13 reveal some variation in ΔM but with much lower gradients with Δz than expected from the *Heath et al.* [1977] data (dashed lines). A further curious feature is that the regression lines pass through $\Delta z = 0$ at around $\Delta M = -2$ kg/cm^2 rather than at the graph origins. The total mass difference of 6 kg/cm^2 over the time 10 to 20 Ma implies that on average there has been a pelagic sediment productivity surplus of 0.6 g/cm^2/ka for the westerly line compared to the easterly line. This result is at odds with the lack of an east-west trend in biogenic silica accumulation [*Leinen*, 1979], which might be expected to reflect primary productivity since silica dissolution is less sensitive to depth.

[22] To compare directly with the Heath et al. data, dissolution rate gradients were calculated from the regressions in Figure 13 and are plotted as horizontal bars in Figure 5. The gray bars in Figure 5 show similar gradients calculated using basement depth as the variable and reveal similar results. Furthermore, the cross symbols ('+') in Figure 5 show gradients calculated from the difference in the carbonate MAR and water depth between DSDP Sites 70 and 575, which verify the trends produced from the seismic data.

5. Sediment Deposition Numerical Model

[23] A numerical model of sediment deposition [*Mitchell*, 1998a] incorporated the high dissolution rate gradients of *Heath et al.* [1977]. We use it here to attempt to simulate the stratigraphy. Mismatches between the seismic and model stratigraphy illustrate how the new seismic data do not allow for such extreme depth-dependent dissolution, and also that MARs from the DSDP drill sites, used in the model, are unrepresentatively large (i.e., reflecting the

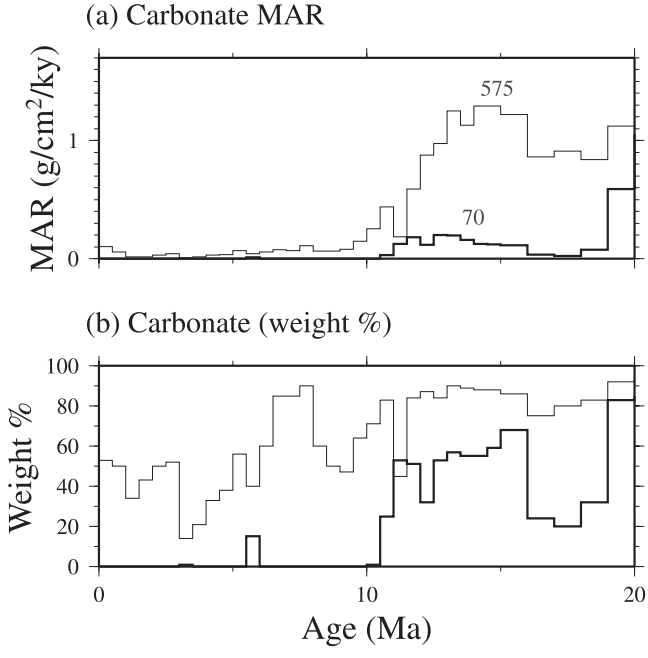

Figure 15. (a) Carbonate mass accumulation rates for DSDP Sites 70 (fine line) and 575 (bold line) from *Lyle* [2003]. The Site 575 curve was derived by combining information from the 575 and 575A cores. (b) Corresponding weight% of carbonate in these sites, showing that the CCD lay above Site 70 and near Site 575 for 0–10 Ma but was below both sites for 10–20 Ma.

general problem of drill sites being located in areas of local deposition).

5.1. Model Description

[24] The sedimentation model is described by *Mitchell* [1998a], but essentially involves backtracking the Pacific tectonic plate in time and, at each time step, accumulating sediment according to a scheme for the mass accumulation rates illustrated in Figure 14. The MAR scheme is based on information from DSDP drill cores, which are used to account for how accumulation rates have varied over time (Figure 14a), with those rates applied to the whole area but adjusted for differences in paleolatitude reflecting equatorial focusing of sedimentation (Figure 14b). Within the model, paleodepth was calculated for each point of the region to account for depth-dependent carbonate dissolution as follows. Paleodepth was estimated allowing for lithospheric subsidence and for the sediment accumulation (Figure 14c). The effect of dissolution in different areas was then calculated by further adjusting the model carbonate MAR using their different paleodepth compared to the reference DSDP Sites 573 and 574 (i.e., if an area had a 100 m greater paleodepth, its carbonate MAR was reduced by 100 m times the dissolution rate gradient in Figure 5 appropriate for that age). The plate tectonic backtracking here was carried out using the *Sager and Pringle* [1988] paleomagnetic apparent polar wander path, which results in approximately 30 km per Ma of northward plate drift for the period 30 Ma to present.

[25] The paleodepth calculation was based on a regression of present-day depths on square root of seafloor age [*Mitchell*, 1998a], because subsidence is different in the equatorial Pacific compared to 'standard' oceanic seafloor [*Parsons and Sclater*, 1977]. One difference between this and the earlier scheme [*Mitchell*, 1998a] is the use of an improved mass accumulation rate model (Figure 14a) from *Lyle* [2003]. The model was run as described by *Mitchell* [1998a], although here we use the model to predict the stratigraphy shown by lower graphs in Figure 9 as well as the total sediment mass.

5.2. Comparisons of Model Predictions to Seismic Data

5.2.1. Suitability of Sites 573 and 574 to Represent Regional Sedimentation

[26] Discrepancies between the model (based on DSDP Sites 573 and 574) and the seismic-derived sediment mass suggest that accumulation rates from the DSDP sites do not represent well the regional sedimentation and further reinforce our argument for a more integrated approach to studying the equatorial sedimentary system. The overall thicknesses of individual sediment intervals in Figure 9 are clearly not compatible with the seismic-derived data, even allowing for distortion between seismic TWT and sediment mass per unit area (e.g., the lavender-red interval is much thicker compared to other intervals in the data than in the model results). The dashed lines in Figure 11 show the bulk MAR computed from the model stratigraphy in Figure 9 and averaged over 0°–5°N in order to represent the regional MAR. The model MAR is clearly larger on average than that derived from the seismic data. Furthermore, the model MAR also has a different structure, even allowing for the conservative estimates of uncertainty in the seismic-derived data (gray areas in Figure 11), so the structure of the mass accumulation rate curve derived from DSDP Sites 573 and 574 (Figure 14a) does not represent well the history of sedimentation at the regional scale. We attribute both the magnitude and structure of the discrepancy mostly to the fact that the DSDP sites were located in areas of relatively thicker sediment. Local thickening of stratigraphy near the base of Site 574 [*Shipley et al.*, 1985] suggests enhanced deposition for the older sediments at that site and numerical analysis of the Site 574 seismic stratigraphy revealed enhanced deposition in basins [*Lagos and Shipley*, 1989], areas where drill sites are typically located. It may also be possible that other less obvious effects of changing local bottom currents over time rendered these sites less representative of the regional sedimentation history.

[27] The problem of local variations in deposition is typical of equatorial Pacific sediments [*Knappenberger*, 2000; *Lagos and Shipley*, 1989] and is best studied with seismic reflection profiles. *Lagos and Shipley* [1989] estimated that downslope transport of sediments from abyssal hills led to higher sedimentation in adjacent valleys by 5–17%, depending on age interval. The generally greater deposition in valleys eventually leads to a smoothing of the abyssal hill topography and a flatter seafloor. Similarly, *Knappenberger* [2000] observed an inverse correlation between height of abyssal hill topography and thickness of seismic units. Because the EW9709 track line crossed the abyssal hill topography at an oblique angle, a periodicity in thickness of units with a wavelength of about 0.5° of latitude was observed.

5.2.2. Dissolution With Depth

[28] For the westerly line at 6°N, the model predicts an abrupt thinning, caused by enhanced carbonate dissolution with depth, that is greater than actually occurs. To compare the shapes of sediment intervals in the model with the seismic-derived data, the model intervals (fine lines in Figure 12) were scaled so as to have the same mean value over 0°–5°N as the data (bold lines in Figure 12 reproduced from Figure 10). This is necessary because of the poor match between data and model absolute mass for selected intervals (Figure 11) and allows the shapes of the graphs at least to be compared. They should be compared ignoring the fine-scale fluctuation which in the model is due to an exaggerated effect of carbonate dissolution caused by the relief in the bathymetry (Figure 7) and in the data is mostly an artifact of local depositional processes.

[29] In the easterly line, sediment older than about 8.55 Ma has roughly comparable decline in mass going north to the model (Figure 12). For sediment younger than 8.55 Ma, the model predicts less deposition around 4°–5°N than actually occurs. In the westerly line (Figure 12), the model generally over-predicts the amount of dissolution going north. This line has the greatest bathymetry gradient (Figure 7), and the over-predicted dissolution is a result of this relief and the large predicted dissolution rates in the model (Figure 5). It

thus illustrates that the dissolution rate gradients of *Heath et al.* [1977] are too large for this part of the Pacific.

6. Discussion

[30] A principal result of this seismic study is that for the period 20 to 10 Ma the difference in carbonate MAR between the two lines suggests a smaller dissolution rate gradient than found by *Heath et al.* [1977]. We note that the dissolution rate gradients derived by *Heath et al.* [1977] did not include much data from north of the equatorial region and none near the westerly seismic line. The *Heath et al.* [1977] data were grouped including sites at different paleolatitude so some of the trends with depth that they observed could represent differences in pelagic productivity. There could also have been local depositional effects as mentioned earlier. However, the seismic derived gradients in Figure 5 are >2 times smaller than the *Heath et al.* [1977] gradients, a discrepancy that is too large to be dismissed as an artifact of the core data. We therefore propose that the central Pacific carbonate system has been asymmetric, with a smaller dissolution rate gradient with depth on the north side of the sediment bulge compared with the south side.

[31] A possible explanation for this asymmetry could lie in this central Pacific region's location at the transition between Pacific Bottom Water with its Antarctic source and Pacific Deep Water, the return flow from the north [*Talley*, 1999]. As the shallower Pacific Deep Water is more corrosive to carbonates than the deeper Antarctic-sourced water mass, there will be a net flattening of the dissolution gradient with depth. This view is supported by a study of *Woodruff and Savin* [1989] who used the ratio of ^{13}C to ^{12}C in benthic foraminifera to trace the progressive aging and oxygen content of bottom waters of the Miocene oceans, based on the assumption that reduced oxygen concentration causes a lowering of $\delta^{13}C$ during oxidation of organic matter. Their results show a similar oceanic structure for the Neogene to the present day, with more oxygen-depleted shallow and intermediate waters in the North Pacific. The transition between oxygen-rich South Pacific and oxygen-poor North Pacific waters occurred at the equator, with North Pacific waters overlying a wedge of oxygen-rich water from the south. We therefore speculate that the boundary between these water masses, and its fluctuation over time, may have contributed to the observed complex pattern of dissolution on the north side of the equatorial Pacific sediment bulge.

[32] Further kinetic and other factors could also complicate the above interpretation. For example, the ratio of organic carbon to inorganic carbon mass accumulation rates (C_{org}/C_{CaCO3}) can have a strong influence on carbonate dissolution [*Archer*, 1991; *Jahnke et al.*, 1997]. Reduced C_{org}/C_{CaCO3} along our westerly seismic line relative to the easterly line would have led to less carbonate dissolution and greater deposition (hence appearing to flatten the dissolution curve), but we know of no evidence for such an east-west gradient in C_{org}/C_{CaCO3} here. Similarly, we know of no evidence that C_{org}/C_{CaCO3} is asymmetric about the equator. Furthermore, whereas organic carbon dissolution effects have been found elsewhere, *Jahnke et al.* [1994] observed no major organic-carbon mediated diagensis in the western equatorial Pacific in an area that should have relatively low C_{org}/C_{CaCO3} as here.

7. Conclusions

[33] This seismic study was intended to illustrate how a spatially continuous stratigraphic database can be useful for systematically characterizing spatial and depth variations in pelagic sedimentary systems. The greater spatial coverage and data volumes allow for averaging over the local variability in sediment deposition that can affect individual drill sites. The seismic data studied here imply that the local variability has a length scale of ~100 km so mass accumulation rates (MARs) derived from drill sites need to be compensated for local effects over this length scale if they are to be representative of regional sedimentation. Specific results of this study include:

[34] 1. Both the seismic data and the numerical model developed using DSDP Sites 573 and 574 show a general decline in the average MAR for the central equatorial region (0°–5°N) from more than 2 g/cm^2/ka prior to 14 Ma to less than 1 g/cm^2/ka at the present day, with a particularly abrupt decline at around 9 Ma. MARs derived using the numerical model are larger than those derived from the seismic data suggesting that DSDP Sites 573 and 574, used in the model, over-represent the amount of pelagic material accumulating in the central Pacific.

[35] 2. Graphs of the sedimentary mass difference (ΔM) and depth difference (Δz) between the two seismic lines at a common latitude show: (1) little dependence of ΔM on Δz for the period 10 Ma to present, as expected given that the CCD lay close to the depth of these lines for this period, (2) a variation of ΔM with Δz for the period 20–10 Ma but with much smaller gradients than *Heath et al.* [1977] derived from DSDP cores for the equatorial and south equatorial regions, and (3), also for 20–10 Ma, offset of the trend of ΔM on Δz away from the graph origin suggesting that there has been an excess of supply by 0.6 g/cm^2/ka on average to the westerly line over this period (a trend that is opposite to that expected). The result (2) suggests that the central Pacific carbonate system has been asymmetric with smaller dissolution rate gradients to the north than south of the equator. A possible explanation could lie in this region's location at the boundary between Pacific Deep Water overlying Antarctic Bottom Water, with the more corrosive Pacific Deep Water causing a flattening of the dissolution trend.

[36] **Acknowledgments.** We thank the officers and crew of the R/V *Maurice Ewing* for their assistance in collecting the seismic data during cruise EW97-09 (NSF grant OCE-9634141). Figures in this paper were prepared with the GMT software system [*Wessel and Smith*, 1991]. I. Hall is thanked for discussions on the Pacific sedimentary regime and two anonymous reviewers are thanked for constructive comments. We gratefully acknowledge JOI/USSAC who provided support to reprocess the seismic reflection data for Leg 199 and digitally archive it. MWL was also partially supported by the NSF-Idaho EPSCoR Program and by the National Science Foundation under award numbers EPS-0132626 and OCE-9907292. NCM was supported by a Royal Society University Research Fellowship.

References

Archer, D., Modeling the calcite lysocline, *J. Geophys. Res.*, *96*, 17,037–17,050, 1991.

Arrhenius, G. A., Pelagic sediments, in *The Sea*, edited by M. N. Hill, pp. 655–727, Wiley-Intersci., New York, 1963.

Berger, W. H., Cenozoic sedimentation in the eastern tropical Pacific, *Bull. Geol. Soc. Am.*, *84*, 1941–1954, 1973.

Berger, W. H., and R. Stax, Neogene carbonate stratigraphy of Ontong Java Plateau (western equatorial Pacific): Three unexpected findings, *Terra Nova*, *6*, 520–534, 1994.

Berger, W. H., and E. L. Winterer, Plate stratigraphy and the fluctuating carbonate line, *Spec. Publ. Int. Assoc. Sedimentol.*, *1*, 11–48, 1974.

Berger, W. H., C. G. Adelseck, and L. A. Mayer, Distribution of carbonate in surface sediments of the Pacific Ocean, *J. Geophys. Res.*, *81*, 2617–2627, 1976.

Berger, W. H., M.-C. Bonneau, and F. L. Parker, Foraminifera on the deep-sea floor: Lysocline and dissolution rate, *Oceanol. Acta*, *5*, 249–258, 1982.

Bloomer, S. F., L. A. Mayer, and T. C. Moore, Seismic stratigraphy of the eastern equatorial Pacific Ocean: Paleoceanographic implications, *Proc. Ocean Drill. Program, Sci. Results*, *138*, 537–553, 1995.

Cande, S. C., and D. V. Kent, Revised calibration of the geomagnetic polarity timescale for the late Cretaceous and Cenozoic, *J. Geophys. Res.*, *100*, 6093–6095, 1995.

Chavez, F. P., and R. T. Barber, An estimate of new production in the equatorial Pacific, *Deep Sea Res.*, *34*, 1229–1243, 1987.

Divins, D. L., and B. Eakins, Total sediment thickness map for the southeast Pacific Ocean, in *International Geological-Geophysical Atlas of the Pacific Ocean*, edited by G. B. Udintsev, Intergov. Oceanogr. Comm., Paris, 1997.

Farrell, J. W, I. Raffi, T. R. Janecek, D. W. Murray, M. Levitan, K. Dadey, K.-C. Emeis, M. Lyle, J.-A. Flores, and S. Hovan, Late Neogene sedimentation patterns in the eastern equatorial Pacific Ocean, *Proc. Ocean Drill. Program, Sci. Results*, *138*, 717–756, 1995.

Heath, G. R., T. C. Moore, and T. H. van Andel, Carbonate accumulation and dissolution in the equatorial Pacific during the past 45 million years, in *The Fate of Fossil Fuel CO_2 in the Oceans*, edited by N. R. Andersen and A. Malahoff, pp. 627–639, Plenum, New York, 1977.

Honjo, S., J. Dymond, R. Collier, and S. J. Manganini, Export production of particles to the interior of the equatorial Pacific Ocean during the 1992 EqPac experiment, *Deep Sea Res.*, *42*, 831–870, 1995.

Jahnke, R. A., D. B. Craven, and J. F. Gaillard, The influence of organic-matter diagenesis on CaCO3 dissolution at the deep-sea floor, *Geochim. Cosmochim. Acta*, *58*, 2799–2809, 1994.

Jahnke, R. A., D. B. Craven, D. C. McCorkle, and C. E. Reimers, CaCO3 dissolution in California continental margin sediments: The influence of organic matter remineralization, *Geochim. Cosmochim. Acta*, *61*, 3587–3604, 1997.

Johnson, D. A., Ocean-floor erosion in the equatorial Pacific, *Geol. Soc. Am. Bull.*, *83*, 3121–3144, 1972.

Kemp, A. E. S., J. G. Baldauf, and R. B. Pearce, Origins and paleoceanographic significance of laminated diatom ooze from the eastern equatorial Pacific, *Proc. Ocean Drill. Program, Sci. Results*, *138*, 641–645, 1995.

Knappenberger, M. B., Sedimentation rates and Pacific plate motion calculated using seismic cross sections of the Neogene equatorial sediment bulge, MS thesis, Boise State Univ., Boise, Idaho, 2000.

Lagos, G. A., and T. H. Shipley, Quantitative estimates of resedimentation in the pelagic sequence of the equatorial Pacific, *Mar. Geol.*, *89*, 269–277, 1989.

Lancelot, Y., Relations entre evolution sedimentaire et tectonique de la plaque Pacifique depuis le Cretace inferieur, *Soc. Geol. Fr. Mem.*, *134*, 1–40, 1978.

Leinen, M., Biogenic silica accumulation in the central equatorial Pacific and its implications for Cenozoic paleoceanography: Summary, *Geol. Soc. Am. Bull.*, *90*, 801–803, 1979.

Lyle, M., Neogenecarbonate burial in the Pacific Ocean, *Paleoceonagraphy*, *18*, doi:10.1029/2002000777, in press, 2003.

Lyle, M., K. Dadey, and J. Farrell, The Late Miocene (11–8 Ma) eastern Pacific carbonate crash: Evidence for reorganization of deep water circulation by the closure of the Panama Gateway, *Proc. Ocean Drill. Program, Sci. Results*, *138*, 821–837, 1995.

Lyle, M., L. Liberty, T. C. Moore, and D. K. Rea, Development of a seismic stratigraphy for the Paleogene sedimentary section, central equatorial Pacific Ocean, *Ocean Drill. Program Init. Rep.*, *199*, 2002a.

Lyle, M. W., et al., Leg 199 preliminary report, Paleogene equatorial transect, 23 October–16 December 2001, Ocean Drill. Program, College Station, Tex., 2002b.

Mayer, L. A., Erosional troughs in deep-sea carbonates and their relationship to basement structure, *Mar. Geol.*, *39*, 59–80, 1981.

Mayer, L. A., T. H. Shipley, F. Theyer, R. H. Wilkens, and E. L. Winterer, Seismic modeling and paleoceanography at deep sea drilling project site 574, *Initial Rep. Deep Sea Drill. Proj.*, *85*, 947–970, 1985.

Mayer, L. A., T. H. Shipley, and E. L. Winterer, Equatorial Pacific seismic reflectors as indicators of global oceanographic events, *Science*, *233*, 761–764, 1986.

Mayer, L.A., et al., *Proceedings of the Ocean Drilling Program, Initial Reports*, vol. 138, Ocean Drill, Program, Tex. A&M Univ., College Station, Tex., 1992.

Mitchell, N. C., Modeling Cenozoic sedimentation in the central equatorial Pacific and implications for true polar wander, *J. Geophys. Res.*, *103*, 17,749–17,766, 1998a.

Mitchell, N. C., Sediment accumulation rates from Deep Tow profiler records and DSDP Leg 70 cores over the Galapagos Spreading Centre, in *Geological Evolution of Ocean Basins: Results From the Ocean Drilling Program*, edited by A. Cramp et al., pp. 199–209, Geol. Soc., London, 1998b.

Muller, R. D., W. R. Roest, J.-Y. Roger, L. M. Gahagan, and J. G. Sclater, Digital isochrons of the world's ocean floor, *J. Geophys. Res.*, *102*, 3211–3214, 1997.

Parsons, B., and J. G. Sclater, An analysis of the variation of ocean floor bathymetry and heat flow with age, *J. Geophys. Res.*, *82*, 803–827, 1977.

Peterson, M. N. A., Calcite: Rates of dissolution in a vertical profile in the central Pacific, *Science*, *154*, 1542–1544, 1966.

Sager, W. W., and M. S. Pringle, Mid-Cretaceous to Early Tertiary apparent polar wander path of the Pacific plate, *J. Geophys. Res.*, *93*, 11,753–11,771, 1988.

Shipley, T. H., E. L. Winterer, M. Goud, S. J. Mills, C. V. Metzler, C. K. Paull, and J. T. Shay, Seabeam bathymetric and water-gun seismic reflection surveys in the equatorial Pacific, *Initial Rep. Deep Sea Drill. Proj.*, *85*, 825–837, 1985.

Talley, L. D., Some aspects of ocean heat transport by the shallow, intermediate, and deep overturning circulations, in *Mechanisms of Millennial-Scale Global Climate Change*, edited by R. S. Webb, P. U. Clark, and L. Keigwin, pp. 1–23, AGU, Washington, D. C., 1999.

Tarduno, J. A., R. A. Duncan, and the Shipboard Scientific Party, Leg 197 preliminary report, motion of the Hawaiian hotspot: A paleomagnetic test, Ocean Drill. Program, College Station, Tex., 2001.

Thunell, R. C., R. S. Keir, and S. Honjo, Carbonate dissolution: An in situ study in the Panama Basin, *Science*, *212*, 659–661, 1981.

van Andel, T. J., G. R. Heath, and T. C. Moore, *Cenozoic Tectonics, Sedimentation, and Paleoceanography of the Central Equatorial Pacific*, 134 pp., Geol. Soc. of Am., Boston, Mass., 1975.

Wessel, P., and L. Kroenke, A geometric technique for relocating hotspots and refining absolute plate motions, *Nature*, *387*, 365–369, 1997.

Wessel, P., and W. H. F. Smith, Free software helps map and display data, *Eos Trans. AGU*, *72*, 441, 1991.

Woodruff, F., and S. M. Savin, Miocene deepwater oceanography, *Paleoceanography*, *4*, 87–140, 1989.

Worsley, T. R., and T. A. Davies, Cenozoic sedimentation in the Pacific Ocean: Steps toward a quantitative evaluation, *J. Sediment. Petrol.*, *49*, 1131–1146, 1979.

M. B. Knappenberger and M. W. Lyle, Center for Geophysical Investigation of the Shallow Subsurface, Boise State University, MS 1536, 1910 University Drive, Boise, ID 83725-1536, USA. (mlyle@cgiss.boisestate.edu; marie.knappenberger@kodak.com)

L. M. Liberty, Research Professor, CGISS/Boise State University, Boise State University, MS 1536, 1910 University Drive, Boise, ID 83725-1536, USA. (lml@cgiss.boisestate.edu)

N. C. Mitchell, Department of Earth Sciences, Cardiff University, P. O. Box 914, Cardiff CF10 3YE, Wales, UK. (neil@ocean.cardiff.ac.uk)